Heliyon 10 (2024) e37967

Contents lists available at ScienceDirect

Heliyon

journal homepage: www.cell.com/heliyon

Review article

Mitigating aerosol-induced respiratory infections in home quarantine: The role of door dynamics and ventilation in residential design

Xunmei Wu [a,b], Mengtao Han [a,b], Hong Chen [a,b,*]

[a] School of Architecture and Urban Planning, Huazhong University of Science and Technology, Wuhan, 430074, PR China
[b] Hubei Engineering and Technology Research Center of Urbanization, Wuhan, 430074, PR China

ARTICLE INFO

Keywords:
Home isolation
Natural ventilation
Exposure risk assessment
Aerosol
LBM-LES
Computational fluid dynamics

ABSTRACT

Respiratory infectious diseases, notably recurring waves of COVID-19 during autumn and winter, have significantly impacted global health and strained public health systems. Home isolation has emerged as a crucial and economical strategy to mitigate these impacts. This study investigates aerosol transmission and infection risks in home isolation environments using the Lattice Boltzmann Method with Large Eddy Simulation (LBM-LES). We focused on the impact of door operations and various natural ventilation rates on aerosol transmission and exposure risk in adjacent rooms. Our findings reveal that, without ventilation, aerosol leakage through door gaps poses a minimal infection risk to adjacent rooms, with an average probability of less than 2×10^{-5}. However, with adequate ventilation, the infection risk for individuals in adjacent rooms for over 3 h can reach 60 %–70 %. Brief door movements have limited impact on infection risk ($p \leq 0.05$, $d \leq 0.20$), with aerosol leakage mainly occurring through door gaps rather than door movements. To reduce cross-infection during home isolation, we recommend avoiding prolonged stays near downwind walls facing the door. This research provides insights into aerosol dynamics in home isolation scenarios, offering theoretical guidance for designing safe isolation spaces and practical advice for healthy family members to minimize infection risk.

Abbreviation Description

ACH	Air Changes per Hour
CFD	Computational Fluid Dynamics
FVM	Finite Volume Method
ID50	Infectious Dose for 50 % of the population
LBE	Lattice Boltzmann Equation
LBM	Lattice Boltzmann Method
LES	Large Eddy Simulation
MRT	Multi-Relaxation Time
NHST	Null Hypothesis Significance Testing
SGS	Sub-Grid Scale
TCID50	Tissue Culture Infectious Dose for 50 % of the population

* Corresponding author. School of Architecture and Urban Planning, Huazhong University of Science and Technology, No. 1037 Luoyu Road, Wuhan City, Hubei Province, PR China.
E-mail address: chhwh@hust.edu.cn (H. Chen).

https://doi.org/10.1016/j.heliyon.2024.e37967
Received 13 June 2024; Received in revised form 12 September 2024; Accepted 14 September 2024
Available online 16 September 2024

Table:

Symbol	Description	Value/Units
f_i	Discrete velocity distribution function	–
x	Position	meters (m)
t	Time	seconds (s)
Δt	Temporal discretization step	seconds (s)
M	Matrix converting distribution function vector from velocity space to moment space vector	–
S	Diagonal matrix	–
ν	Viscosity coefficient	$\frac{1}{3}\left(\frac{1}{S_9}-\frac{1}{2}\right)\mathrm{m}^2/\mathrm{s}$
ν_t	Subgrid scale viscosity	m^2/s
ν_0	Laminar viscosity	m^2/s
C_s	Smagorinsky parameter	–
Δ	Filtering scale	meters (m)
ρ	Fluid density	kilograms per cubic meter $(\mathrm{kg}/\mathrm{m}^3)$
u	Velocity	meters per second (m/s)
C_i	Concentration of aerosol i	particles per cubic meter (particles $/\mathrm{m}^3$)
$v_{s,i}$	Aerosol settling velocity	meters per second (m/s)
$\epsilon_{p,i}$	Aerosol eddy diffusivity	m^2/s
D_i	Brownian diffusion coefficient	m^2/s
$S_{d,i}$	Sink term for the deposition of aerosol i	particles per cubic meter per second (particles $/\mathrm{m}^3/s$)
$v_{d,i}$	Local deposition velocity	meters per second (m/s)
A_w	Face normal vector	–
$V_{\mathrm{cell},i}$	Grid cell volume	cubic meters (m^3)
$C_{w,i}$	Local concentration of the near-wall cell	particles per cubic meter (particles $/\mathrm{m}^3$)

1. Introduction

In recent years, infectious respiratory diseases such as COVID-19 and influenza A have become increasingly serious public health concerns. These diseases possess high transmission capabilities and can spread rapidly through the air, leading to severe illness and even death, particularly among high-risk populations [1]. Given that individuals spend a significant portion of their time indoors, it is crucial to gain a comprehensive understanding of the transmission processes and mechanisms of these diseases and implement effective measures to prevent their indoor spread [2].

Home isolation is a widely employed measure to control the transmission of infectious diseases by reducing interpersonal contacts and minimizing interactions between infected individuals and susceptible individuals, thus effectively curbing the spread of viruses or bacteria [3]. To gain a comprehensive understanding of how to mitigate disease transmission during home isolation, a review of previous literature offers valuable insights and serves as a foundation for formulating effective strategies. Notably, the role of aerosol transmission within indoor environments is critical, as demonstrated by several key studies. Morawska et al. have detailed the mechanics of aerosol generation and dispersal within residential settings, highlighting the potential for significant airborne transmission of pathogens [4–6]. Similarly, research by Liu et al. underscores the persistence and concentration of airborne particles in confined spaces, further stressing the importance of ventilation systems in mitigating risk [7]. Furthermore, a study by Nicas et al. explores the quantitative framework for the infection risk of aerosols in various indoor scenarios, providing essential insights into effective isolation strategies [8–10]. Our study builds on this collective body of knowledge by focusing specifically on the role of door operations and door gaps in aerosol transmission during home isolation. Cava et al., explored the experiences of home isolation during the 2003 outbreak of Severe Acute Respiratory Syndrome (SARS) in Toronto [11]. Elgendy et al., investigated the knowledge and adherence to home isolation guidelines among COVID-19 patients and their close contacts [12]. Their findings revealed a satisfactory level of awareness and compliance with home isolation guidelines among individuals affected by COVID-19. Guo et al., developed an individual-based computational model to simulate the occurrence, infection, detection, isolation, and release (recovery) processes of asymptomatic SARS-CoV-2 infections or patients within a community setting [13]. Zhang et al., constructed a stochastic discrete model focused on the 2021 COVID-19 outbreak in Guangzhou to compare the efficacy of centralized quarantine and mandatory home isolation measures [14]. T However, our study differs by using the Lattice Boltzmann Method with Large Eddy Simulation (LBM-LES) to model the specific impact of door gaps and movements under various natural ventilation rates.

However, during home isolation, the opening and closing of isolation room door and the gap between the door leaf and the floor can potentially increase the risk of infection [15]. When the door is frequently opened and closed, it may induce airflow, allowing viruses or bacteria to spread from the isolation area to other areas. Additionally, the door gap can serve as a pathway for the transmission of pathogenic aerosols, further increasing the risk of infection among household members [16]. Therefore, it is important to understand the research on the impact of the door gap on the leakage of contaminants. For example, studies have investigated the infiltration of pollutants caused by the opening and closing of the door and the door gap in various environments [17–20]. Exploring the principles and factors influencing the dispersion of contaminants caused by door gap can provide scientific evidence for designing and improving ventilation and air purification systems in buildings. This knowledge has significant practical applications in the context of home isolation, laboratories, and healthcare facilities.

The Lattice Boltzmann Method with Large Eddy Simulation (LBM-LES) is an advanced computational fluid dynamics technique that

combines the advantages of LBM and LES to achieve high-precision and efficient simulation of complex flow phenomena [21]. In the field of indoor ventilation research, LBM-LES has demonstrated significant advantages in simulating detailed flow structures and turbulent characteristics involved in aerosol transmission within complex indoor environments. For example, Sajjadi et al., utilized LES, RANS, and hybrid RANS/LES turbulence models within the LBM framework to study turbulent indoor airflow, specifically simulating airflow patterns around human bodies using the MRT-LBM approach [22]. Han et al., discussed the effectiveness of a novel wall treatment method based on LBM-LES in predicting indoor and outdoor airflow in building environments [23]. Chen et al., discussed the application of unique boundary conditions in LBM in the field of building environment [24]. These studies demonstrate the wide application prospects of the LBM-LES method in the fields of indoor ventilation and infectious disease transmission research. Therefore, this study will utilize the LBM-LES method for simulation research.

The objective of this study is to investigate the influence of the isolation room door on aerosol transmission and exposure risk in the home isolation environment under different natural ventilation rates using the LBM-LES method. The research methodology comprises several sequential steps. The research methodology comprises several sequential steps.

Firstly, the reliability of the LBM-LES method is ensured through validation, as detailed in Appendix A. Subsequently, the indoor environment of a typical residential layout in Wuhan is modeled and transient simulations are conducted using the LBM-LES method. The simulations encompass various indoor ventilation scenarios under different natural ventilation rates, including leaks caused by prolonged closure of the room door and leaks occurring during the door opening and closing process. Next, the infection risk is assessed based on the simulation results. Finally, appropriate guidelines for indoor activities and architectural layout design are provided based on the evaluation outcomes. These steps interconnect to form a cohesive research approach, from validating the method, modeling the environment, conducting simulations, assessing risks, and providing practical recommendations.

This study's key significance lies in its deep exploration of aerosol transmission paths and infection risks within home isolation environments, focusing on creating safe isolation spaces at home. By determining appropriate ventilation conditions and door usage, we aim to control aerosol transmission. Additionally, the research provides practical guidance for healthy family members to avoid infection from isolated individuals.

2. Methodology

This diagram outlines the methodology of a study on aerosol dynamics and infection risk assessment using various computational and statistical methods. It starts with the Multi-Relaxation Time Lattice Boltzmann Equation (MRT-LBE) method for fluid dynamics simulations, followed by aerosol calculations using a Drift Flux Model. The statistical analysis section includes the Wilcoxon Rank-Sum Test and Cliff's Delta for assessing ventilation scenarios, and a dose-response model to evaluate infection risks, culminating in the development of a risk matrix. This approach integrates theoretical modeling and practical assessments to study indoor air quality and its health impacts.

2.1. Overview of the MRT-LBE method

We selected the LBM-LES method because it combines the high accuracy of capturing turbulent flows with the computational efficiency and flexibility needed to handle complex indoor geometries and boundary conditions. This method is particularly effective for detailed simulations of aerosol transmission, allowing us to accurately model the intricate flow dynamics and aerosol dispersion patterns in home isolation scenarios, which are essential for understanding and mitigating infection risks.

The Lattice Boltzmann Equation (LBE) is a method that models fluid flows based on kinetic theory and the Boltzmann formula, as opposed to the conventional method of solving the Navier-Stokes equations directly [25]. The LBE monitors the evolution of the discrete velocity distribution function $f_i(x,t)$ at a position x and time t, using a Multi-Relaxation Time (MRT) collision model, as described by equation (1) [26]:

$$f(x + c_i\Delta t, t + \Delta t) = f(x,t) - \mathbf{M}^{-1}S[m - m^{eq}]\Delta t \tag{1}$$

where Δt is the temporal discretization step, $\mathbf{M}$ is a matrix that converts the distribution function vector f from the velocity space to a moment space vector m, and S is a diagonal matrix obtained according to equation (2). The viscosity coefficient v can be calculated using equation (3).

$$\mathbf{S} = \mathrm{diag}(0, S_1, S_2, 0, S_4, 0, S_4, 0, S_4, S_9, S_{10}, S_9, S_{10}, S_{13}, S_{13}, S_{13}, S_{16}, S_{16}, S_{16}) \tag{2}$$

$$v = \frac{1}{3}\left(\frac{1}{s_9} - \frac{1}{2}\right) = \frac{1}{3}\left(\frac{1}{s_{13}} - \frac{1}{2}\right) \tag{3}$$

To simulate turbulent motions at high Reynolds numbers, the Lattice Boltzmann-Multi-Relaxation Time (LBM-MRT) method can be combined with a Large Eddy Simulation (LES) subgrid model [27]. In this paper, the commonly used Smagorinsky eddy viscosity model is adopted. The viscosity coefficient is adjusted by adding the subgrid scale viscosity v_t to the laminar viscosity v_0, as described by equation (4). The turbulent viscosity v_t is determined by the Smagorinsky parameter C_s, the modulus of the strain rate tensor $|\mathbf{S}|$, and the filtering scale Δ, as described by equation (5).

$$v = v_0 + v_t \tag{4}$$

$$\nu_{sgs} = (C_s\Delta)^2|\mathbf{S}| \tag{5}$$

The zero- and first-order moments of f_i are the fluid density ρ and velocity u, respectively, as described by equations (6) and (7).

$$\rho(x,t) = \sum_i f_i(x,t) \tag{6}$$

$$\rho u(x,t) = \sum_i c_i f_i(x,t) \tag{7}$$

2.2. Drift flux model for aerosol calculation

We use a drift flux model developed based on the Euler method and apply it into LBM method to numerically describe the migration of aerosol in indoor environments [28]. The transport equation (8) considering the removal mechanisms of turbulent diffusion, sedimentation rate of aerosol in the air can be written as:

$$\frac{\partial C_i}{\partial t} + \nabla\cdot\left[(\mathbf{u}+\mathbf{v}_{s,i})C_i\right] = \nabla\cdot\left[(D_i+\varepsilon_{p,i})\nabla C_i\right] + S_{d,i} \tag{8}$$

where C_i is the concentration of aerosol i, $\boldsymbol{v_{s,i}}$ is the aerosol settling velocity, $\varepsilon_{p,i}$ is the aerosol eddy diffusivity, D_i is the Brownian diffusion coefficient, and $S_{d,i}$ is the sink term for the deposition of aerosol i and it is expressed as:

$$S_{d,i} = -\frac{\sum(\mathbf{v}_{d,i}\cdot\mathbf{A}_w)}{V_{cell,i}}C_{w,i} \tag{9}$$

where the summation in parentheses is over all wall faces of the first layer grids near the wall; $v_{d,i}$ is the local deposition velocity, which was evaluated using the method suggested by Lai and Nazaroff [29]; A_w is the face normal vector; $V_{cell,i}$ is the grid cell volume; and $C_{w,i}$ is the local concentration of the near-wall cell. The deposition of bacteria onto the wall surface has been included in the deposition sink term (Eq. (9)).

In the model, heat and humidity, air temperature, and relative humidity within the test chamber were assumed constant, and heat and moisture transfers were not included.

2.3. Wilcoxon rank-sum test and Cliff's delta

We use the Null Hypothesis Significance Testing (NHST) to evaluate the impact of different operating scenarios (door opening and closing and different ventilation rates) on pollutant release during the experiment [30]. The analysis depends on the sample size and the size of the effect. This study uses two non-parametric statistical tests to analyze the differences in concentration of the flow field specific regions between different ventilation scenarios and the door opening process: (i) Wilcoxon rank-sum test (i.e. *U* test); (ii) Cliff's Delta. The *U* test is used to compare if the overall mean ranks of two samples are different [31]. A p-value $\leq$0.05 indicates rejection of the null hypothesis (i.e. no difference) and acceptance of the alternative hypothesis. Cliff's Delta is a measure of effect size used to quantify the difference between two populations beyond the interpretation of the p-value [32]. The results of the effect size are interpreted by the absolute value |d|, including negligible (|d|<0.147), small (0.147$\leq$|d|<0.33), moderate (0.33$\leq$|d|<0.474), and large (0.474$\leq$|d|).

Table 1
Variables and Parameters in Dose-response model.

Parameters	Description	Specific Value or Equation
c	Pathogen content in the saliva or phlegm produced by respiration, obtained from large-scale patient samples. It's measured in units of TCID50, which is the average dose causing infection in 50 % of the population through tissue culture [36].	10^5 $TCID_{50}$/ml
$f(t)$	Viability function representing the changing activity of viruses or bacteria in the aerosol over time [37].	$f(t) = 0.0351e^{-0.261t}$
m	Number of spatial divisions in the fluid.	–
j	A certain segment in the space	–
β_j	Size-specific settling rate of the aerosol in the respiratory tract for the j-th division [38].	$\beta = 0.6$
r_j	Fitting parameter that makes $P_1(t_0) = 0.5$ when the infection dose is ID50, representing the infectiveness of the aerosol in the respiratory tract for the j-th division [38].	$r = 0.385$
q	Exhalation frequency	–
p	Pulmonary ventilation rate of the susceptible person, assumed to be a relatively inactive group with a metabolic rate of 1.2 [39].	–
t_0	Exposure time.	–
$v(t)_j$	Volume density of the aerosol, normalized with the average initial aerosol concentration measured at the mouth [40].	0.092/cm^3

2.4. Infection risk assessment: dose-response model

A dose-response model is a statistical model used to link exposure to a treatment or intervention to the response or outcome [33]. It is widely used in fields like pharmacology, toxicology, and environmental health to study the impact of substances on living organisms. To build a dose-response model, large-scale experiments are needed to determine the relationship between the pathogenic dose and infection risk of a pathogen. The ID50, or the dose at which 50 % of the population is infected, is used to define this relationship [34]. improved the basic dose-response model by including factors like aerosol size and spatial heterogeneity. They developed a formula to predict the time-varying infection risk of individuals in different states (stationary or moving).

$$P_1(t_0) = 1 - \exp\left(-\sum_{j=1}^{m} r_j \beta_j cpqt_0 \int_0^{t_0} v(t)_j f(t) dt \right) \tag{10}$$

This paper calculates the time-varying infection risk based on the more mature model for influenza A, with specific parameter values taken from Ref. [35]. Please refer to Table 1 for specific value.

In this study, a risk matrix is established to evaluate the infection risk by incorporating both the likelihood of the risk event and its potential impacts. The risk, probability, and consequence levels are expert-determined and categorized into five intervals based on a score range of 0–10. The consequence of the event is quantified through the average infection probability among susceptible individuals in indoor environments, which serves as the basis for classifying the level of consequences, as presented in Table 2 [41].

3. CFD setups in numerical modeling

3.1. Simulation setup

3.1.1. Typical residential layouts selection

This study applies architectural typology principles to analyze residential unit layouts in Wuhan, Hubei Province, China, spanning 2014 to 2024. Initially, a survey was conducted to assess housing preferences across various age groups, focusing on internal living area, room types, and environmental factors. The analysis identified three popular layouts: two-bedroom with one living room, three-bedroom with two living rooms, and four bedroom with two living rooms, with a particular demand for south-facing three-bedroom units.

Images of these units were collected across 13 administrative districts and 77 neighborhoods in Wuhan, totaling 198 units, of which 63 met the survey criteria and were included in the dataset. Urban residential designs tend to show significant similarities due to standardized design methods, reflecting a maturity in layout configurations.

The study employs similarity theory to systematically select typical unit types based on a mathematical statistical analysis of features like geometric dimensions, form indices, the number of bays and depth units, and total floor area. This approach uses the mean as a similarity parameter to gauge the distribution of features across units, identifying those with the most concentrated similarity for further analysis. The findings are summarized in Table 3.

This study utilized clustering algorithms to analyze residential layouts in recent year constructed residence buildings in Wuhan, aiming to identify representative types for urban planning and design. During the data preprocessing stage, collected layout data were standardized to ensure balanced influence across each feature dimension. Feature selection focused on key factors affecting comfort and spatial functionality, such as interior living area, orientation, unit depth, and the number of partitions. The K-means clustering algorithm [42] was employed, involving random selection of K cluster centers and iterative updating of these centers based on minimizing the Euclidean distance between each point and its cluster center, until the clustering results stabilized. Multiple experiments determined that K = 5 is the optimal number of clusters, as it adequately reflects the diversity and inherent patterns of the housing types.

The clustering revealed common characteristics: interior areas ranging from 89 to 127 square meters, 2–3 bays on both the north and south sides, and unit depths of 2–3. Room distribution included two rooms along the depth (west outer wall) and a total of 3–4 rooms in depth, with 1–2 partitions in the living and master bedrooms. These findings reflect market demands and contemporary design trends, emphasizing aspects such as sunlight, ventilation, and privacy.(see Fig. 1)

3.1.2. Computational domain description

Based on the clustering analysis described previously, this study identified the fundamental characteristics of typical residential units in Wuhan. A residential layout that exhibits these characteristics was selected as the subject of our study (see Fig. 2(a) and (b)).

Table 2
Consequence level and score based on infection probability.

Infection probability *P*/%	Probability level	Acceptable level
<15	Extremely Low Probability of Occurrence	Negligible
15–30	Low Probability of Occurrence	Partially Acceptable
30–60	High Probability of Occurrence	Unacceptable
>60	Extremely High Probability of Occurrence	Unacceptable

Table 3
Similar characteristics of unit types to be surveyed.

m1	m2	m3	m4	m5	m6	m7	m8	m9
Interior Area (m^2)	North-facing Bay	South-facing Bay	Unit Depth	North-facing Bay Number	Depth-direction Rooms (west outer wall)	Depth-direction Rooms (all bays)	Living Room Openings Count	Master Bedroom Openings Count

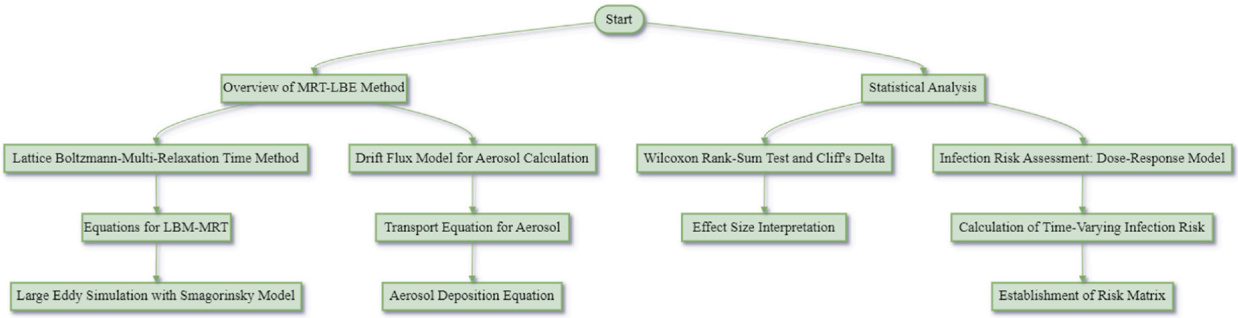

Fig. 1. Methodology diagram.

This layout is a well-regarded residential unit situated in Wuhan, Hubei Province, China. Notably, it was acclaimed as one of the top ten residential designs in 2022. The residential unit is south-facing and adjacent to a street, consisting of three bedrooms, one dining room, one living room, and two bathrooms, with a total floor area of approximately 100 square meters. The master bedroom, situated on the southern side, has an en-suite bathroom, making it suitable for home isolation [43].

To simulate a realistic home isolation scenario, this study assumes the presence of an individual infected with influenza A, who remains in a prone position on the bed in the master bedroom for an extended period. The individual's mouth serves as the source of pathogens; however, the geometric complexity of the human body is not considered in the calculations.

A sliding window is present on the southern wall of the residential unit. Assuming a constant outdoor wind speed, the patient can control the ventilation rate inside the room by adjusting the opening size of the sliding window. It is assumed that the door to the en-suite bathroom within the master bedroom remains closed, and there is only a small gap between the master bedroom and the bathroom. When the door between the master bedroom and the dining room/living room is closed, the two rooms are connected through a small gap, which is the main focus of this study.

The computational domain is set within the red boundary shown in Fig. 2(a), including the master bedroom (excluding the bathroom), the living room, and the dining room. The living room is connected to an open balcony through a floor-to-ceiling sliding door, which can only be opened up to 50 % of its total area. This study assumes that the door remains half-open on the western side for an extended period.

In this research, particular attention is given to the area enclosed by the blue dashed lines ($0.7m < z < 1.6m$), which corresponds to the commonly occupied and active regions, commonly referred to as the breathing zone. These areas, including the living room (Livingroom), dining room (Diningroom), the vicinity of the master bedroom door (Neardoor), and the overall outside area of the master bedroom (Outroom), constitute the main focus of our study investigation. To further analyze and understand individual exposure and infection risks within different regions, three sensors are placed in various locations inside and outside the bedroom. By collecting data from these sensors, This study can conduct in-depth research and quantification of potential infection risks in different environmental and spatial settings.

3.2. Boundary conditions and case setting

Within the computational domain, there are two windows on the same side of the building. Typically, the wind pressure on the same wall side remains relatively consistent; however, in this layout, due to the balcony's influence on airflow disturbance [44], the sliding doors in the Livingroom experience a relative negative pressure compared to the sliding windows in the bedroom. Consequently, the overall airflow direction within the home is from the bedroom towards the living room. To validate this conclusion, the residential unit was placed in an idealized urban block for CFD simulation, which confirmed the scientific validity of these results [45]. Additionally, the average pressure difference between the two windows was used to estimate an entrance wind speed of approximately 0.1012 m/s (Appendix B).

Additionally, based on the study by Xiong et al. [50], the window airflow velocity in a single-sided ventilated room adjacent to a street canyon in Wuhan, under strong outdoor wind conditions (wind speed of 3 m/s), was found to be 0.1008 m/s, which is very close to the wind speed calculated based on the pressure difference between the inlet and outlet (0.1012 m/s). Therefore, this study believe that this inlet boundary condition is in line with physical reality. This airflow velocity is considered as a constant value for the master bedroom window in this study. According to the "Code for Design of Civil Buildings Heating, Ventilation and Air Conditioning (GB

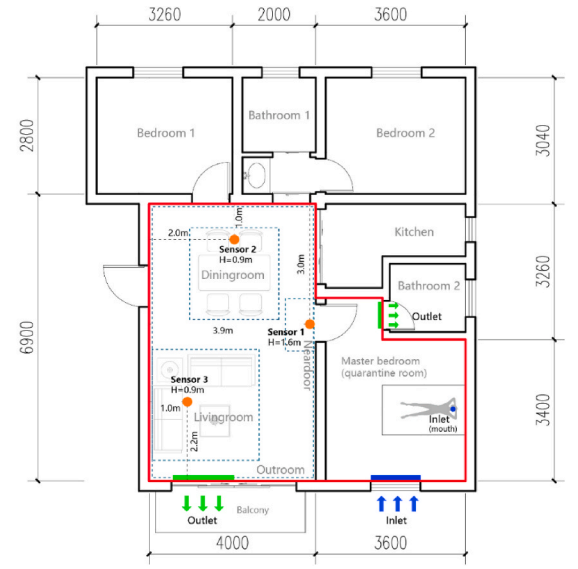

(a) 2D Floor Plan

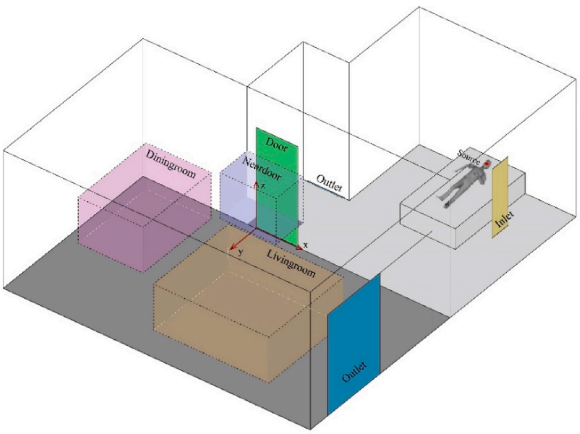

(b) 3D Schematic Diagram

Fig. 2. Schematic diagram of the computational domain.

50736-2012) ," the air exchange rate in a bedroom should not be less than 0.75 air changes per hour (ACH). Moreover, previous research suggests that an air exchange rate of more than 6 ACH per hour can effectively reduce the persistence of the coronavirus in indoor spaces [16]. Therefore, the indoor air exchange rate is set within the range of 0.75–6 h^{-1}. The mouth and nose are simplified as a 3 cm diameter circle, and the breathing velocity at the mouth is modeled as a sine function. To simulate realistic breathing

Table 4
Standard calculation conditions.

Items	Content
Number of grids	0.68 million (approximately)
SGS model	WALE [46]
Inflow	Velocity inlet; U = 0.1008 m/s
Outflow	Zero-gradient condition
Pollution source	Velocity inlet; U = 1.66 * sin (2 * pi *t/15) m/s [27]; c = 0.092/cm^3 [40]
Aerosol size	Dp = 10^{-6} m [47]
Wall & Ground	No-slip wall with wall function [23]
Relaxation time scheme	MRT [48]
Collision model	D3Q19 [49]

conditions, the maximum exhalation velocity is set to 1.66 m/s [51], the aerosol concentration at the mouth is 0.092/cm3 [40], and the breathing frequency is 15 breaths per minute [39]. There are two outlet boundaries, namely, the door gap connecting the master bedroom and the bathroom, and the western half of the sliding door in the living room, which are set as outflow boundaries. The door gap size connecting the master bedroom and bathroom is 0.8 * 0.03m, and the door gap size connecting the living room, dining room, and master bedroom is 0.6 * 0.03m. Specific computational parameters are provided in Table 4.

In certain scenarios involving a series of actions such as opening, staying, and closing the door, they are set as uniformly opening the door (with a duration of 4 s and an angle of 45°), staying for 7 s, and closing the door (with a duration of 4 s and an angle of 45°). The specific scenario settings are shown in Fig. 3 [17]. The initial flow field for cases 2 to 9 is obtained from the computation result of case 1. Taking case 2 as an example, the calculation starts from all windows closed and natural breathing of the human body (natural aerosol transmission) and continues for 12 h until the flow field reaches a steady state (case 1). Subsequently, the master bedroom window is opened to ensure an air exchange rate of 0.75. A series of open-stay-close door actions (approximately 15 s) are performed, and the computation continues for 2 h. The other scenarios are conducted in a similar manner.

4. Result and discussion

4.1. Door gap leakage with no ventilation

Under conditions of prolonged ventilation absence, the leakage of aerosols through the door gap is negligible compared to the aerosol exhaled from the mouth, as shown in Fig. 4(a), and Inroom refers to the space within the quarantine room and Outroom refers to spaces in dining room and living room (outside the quarantine room). In this case, the primary manifestation in the isolation room is the accumulation effect of aerosols. Throughout this period, the average relative aerosol concentration outside the isolation room remains at a low level (<0.04).

Compared to the Diningroom and the Neardoor, the accumulation effect of aerosols in the Livingroom area begins earlier, as depicted in Fig. 4(b). This earlier accumulation is attributed to the Livingroom's proximity to large wall surfaces, which facilitates aerosol deposition and retention. The walls create a barrier that limits airflow, allowing aerosols to settle more quickly in this area.

However, in the Neardoor space, the airflow diffusion direction is more open, which hinders aerosol accumulation. The open airflow in this region promotes dispersion and reduces the likelihood of particles settling, delaying the accumulation effect.

Although different regions exhibit variations in the initiation time of aerosol accumulation, the aggregation rate remains similar across all areas. This consistency in the aggregation rate indicates that while initial accumulation times vary due to local airflow conditions and physical barriers, the overall dynamics of aerosol aggregation follow a comparable pattern once initiated.

Based on the time-averaged analysis of the aerosol concentration in the flow field, Fig. 5(a)–(d) show the streamlines and concentration distribution in different planes, significant aerosol accumulation effects are observed on the west wall and floor. Specifically, the central region of the west wall exhibits the highest relative aerosol concentration in the external isolation room. This phenomenon is primarily attributed to the airflow discharged through the door gap, which generates a clockwise perturbation flow field outside the isolation room. Simultaneously influenced by wall surfaces and gravity, the airflow velocity in this region decreases. From a planar perspective, the airflow forms a clockwise and counterclockwise vortex motion in the north and south sides of the dining

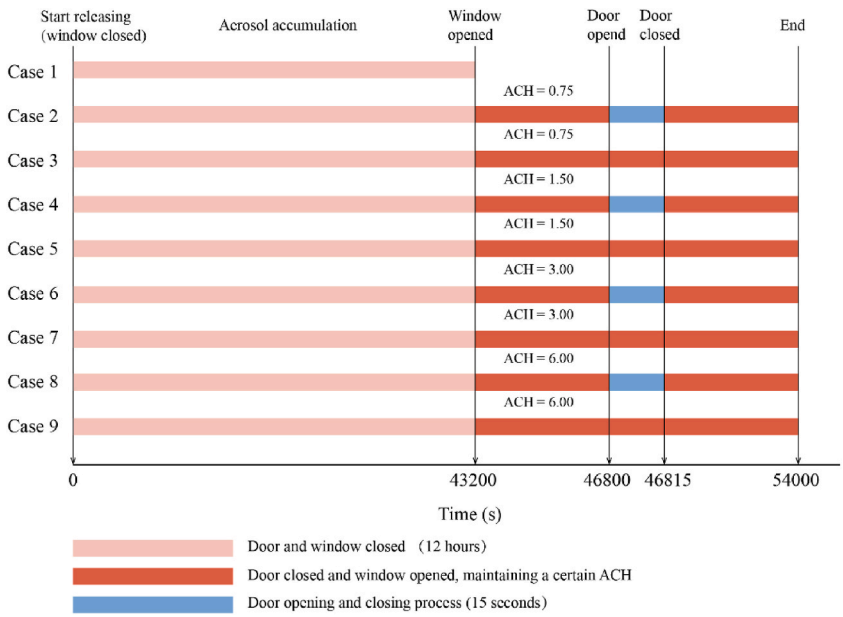

Fig. 3. Case settings.

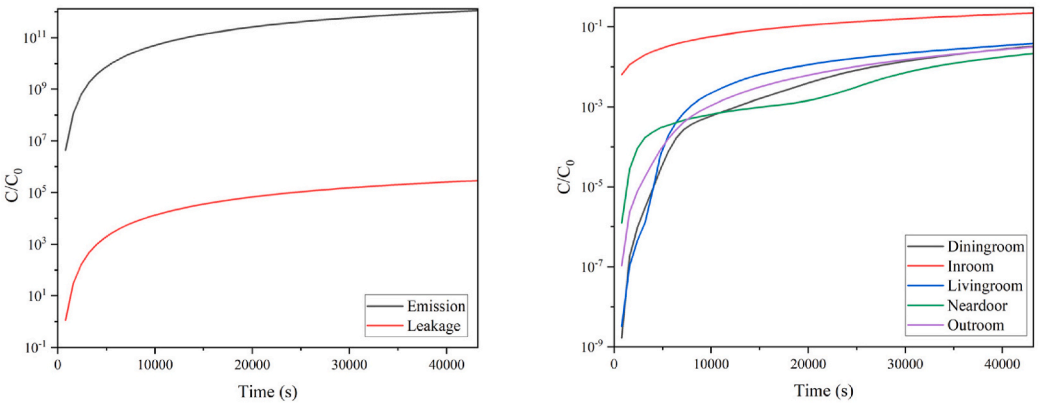

(a) Emission of Pollutants from the Mouth and Leakage through Door Gaps

(b) Relative Average Concentrations in Regions

Fig. 4. Pollutant Leakage and Its distribution in Key Regions (The start time corresponds to the start time in cases above).

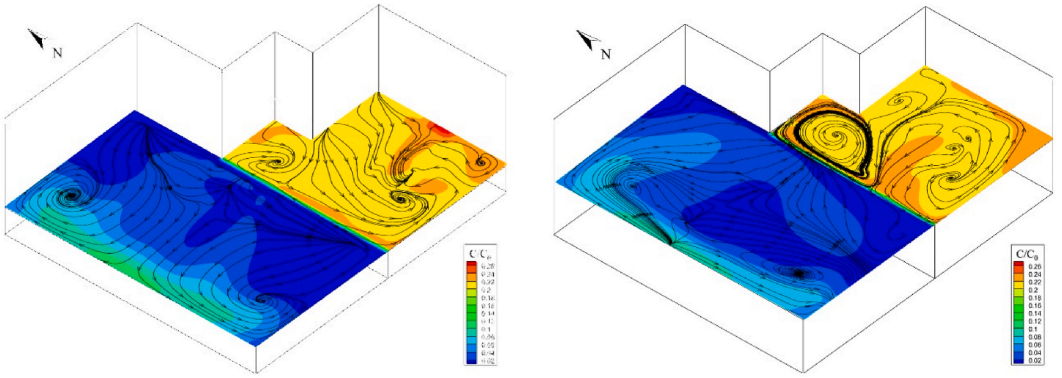

(a) Streamlines and Concentration Distribution at z =0.7m

(b) Streamlines and Concentration Distribution at z=1.5m

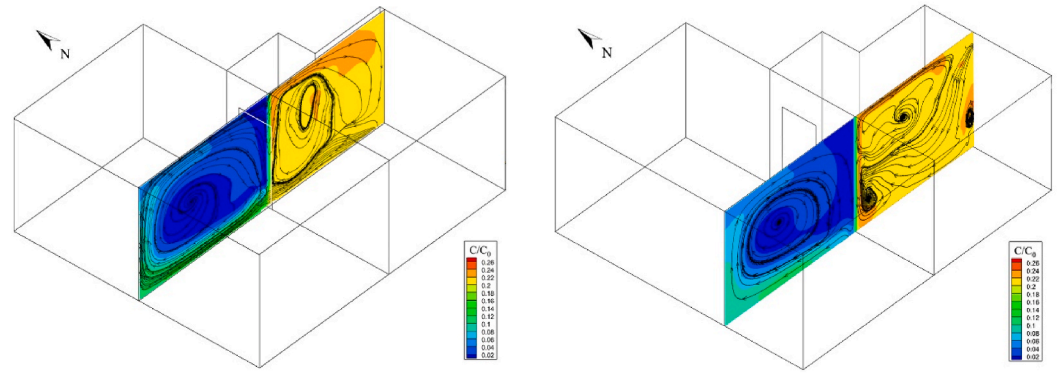

(c) Streamlines and Concentration Distribution at x=1m

(d) Streamlines and Concentration Distribution at x=2m

Fig. 5. Streamlines and concentration distribution at various sections.

room and living room, respectively. At the intersection of these two vortices, the airflow velocity is relatively slow in the central region of the west wall, leading to aerosol accumulation in that area.

4.2. The impact of natural ventilation rates

4.2.1. The impact of ventilation rates on door gap leakage

Fig. 6(a)–(d) presents the average concentration in different respiratory zones under different ventilation rates, the t = 0 here represents t = 43200s as shown in Fig. 3, which means adding different ventilation rates (without opening or closing doors) after 43200s without ventilation. During the initial period of window opening, the sudden increase in ventilation rate results in a pronounced aerosol transport effect, leading to one or more peaks in the outside aerosol concentration. A higher ventilation rate results in an earlier occurrence of peaks in aerosol concentration, and when the ventilation rate is kept constant, the peaks and troughs are more closely aligned with the ventilation rate.

In cases with higher ventilation rates (such as case 5, case 7, and case 9), the peaks in aerosol concentration end before 4000s, followed by a gradual decrease in concentration, indicating that ventilation primarily acts as a means of aerosol clearance. When the ventilation rate is set at 3 or 6 air changes per hour (case 7 and case 9), the leakage through the door gap in different zones exhibits similar characteristics, with aerosol concentrations stabilizing around 0.04. This suggests that when the ventilation rate exceeds 3, the aerosol leakage through the door gap starts to exhibit similar features. However, under lower ventilation rates (such as case 3), the peak in aerosol concentration is less prominent, indicating that aerosol leakage through the door gap in the Outroom continues to accumulate, showing a gradual increasing trend.

It is evident that, in the presence of ventilation in the isolation room, there is a certain degree of aerosol leakage from the outer environment. The average peak relative concentration of outdoor pollution is approximately 0.075, which occurs briefly after window opening and gradually dilutes to around 0.04. Under higher ventilation rates, both the accumulation and clearance cycles of aerosols are relatively short. However, under lower ventilation rates, the outer environment can maintain a relatively high aerosol concentration over an extended period. Based on our findings, when designing isolation rooms for epidemic prevention purposes, it is crucial to minimize the size of the door gap to reduce aerosol leakage. Our simulations suggest that even small gaps can lead to significant aerosol transfer, especially at lower ventilation rates. To optimize door gap sizes, it is recommended to keep gaps as narrow as possible,

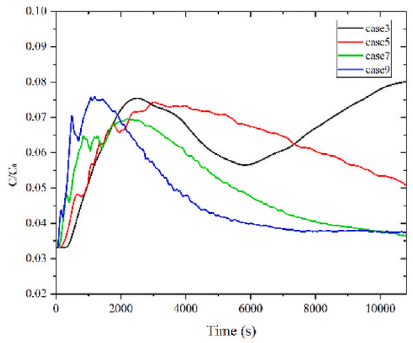

(a) The average concentration in the Diningroom with time variety

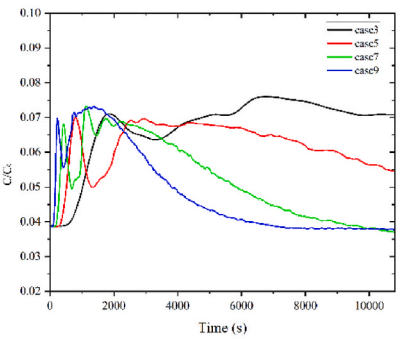

(b) The average concentration in the Livingroom with time variety

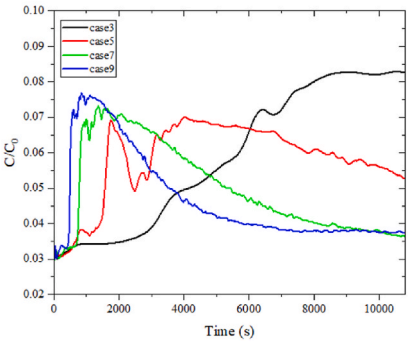

(c) The average concentration in the Neardoor with time variety

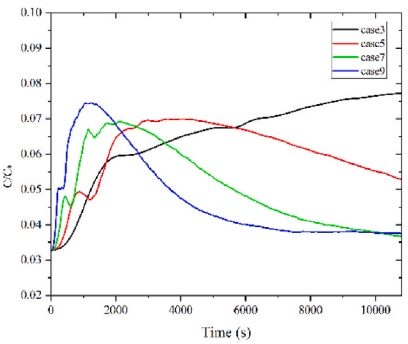

(d) The average concentration in the Outroom with time variety

Fig. 6. The average concentration in different respiratory zones for different ventilation rates with time variety (The start time corresponds to the t = 43200 in cases above).

ideally less than 3 mm, while ensuring that the door can still function properly. Additionally, maintaining a ventilation rate of at least 3 air changes per hour within the isolation room can help mitigate aerosol accumulation and reduce infection risk.

4.2.2. The impact of ventilation rates on door opening leakage

By comparing the effects of door opening and closing under the same ventilation rates, this study observed significant differences in the manner and magnitude of their impact on the airflow field, the t = 0 here represents t = 43200s as shown in Fig. 3, which means adding different ventilation rates without opening or closing door after 43200s without ventilation. Among the sensors, sensor 1, which is located closer to the door, exhibited the highest sensitivity to changes in the airflow resulting from door operations. Therefore, our study analysis was primarily based on the data collected from sensor 1. To mitigate the potential influence of consistent data before performing door operations (prior to 3600s), This study focused on statistical analysis within the timeframe of 3600s–10800s.

In cases 2 and 3, the door operations initiated at 3600s resulted in significant indoor aerosol leakage, with sensor 1 exhibiting multiple distinct peaks in aerosol concentration, approximately three times higher than the leakage value through the door gap. The aerosol leakage caused by door operations took approximately 3000s to be cleared. Therefore, under lower ventilation rates, the door operations have a substantial impact on the airflow field ($p \leq 0.05$, $|d| \geq 0.474$). Individuals from the outdoor environment should avoid approaching the isolation room door during the short period following door operations when the ventilation rate is low (as shown in Fig. 7(a)).

When the ventilation rate is set at 1.5 air changes per hour (as shown in Fig. 7(b)), the door operations have a significant impact on the airflow field, but the magnitude of the impact is moderate ($p \leq 0.05$, $|d| \leq 0.33$). At a ventilation rate of 3 air changes per hour (as shown in Fig. 7(c)), opening the door results in aerosol dilution, leading to a temporary and pronounced decrease in aerosol concentration at the monitoring point. This is because, under higher ventilation rates, the aerosol concentration inside the isolation room is similar to that of the outdoor environment, and opening the door allows the aerosols accumulated near the door to disperse rapidly, resulting in a transient dilution effect ($p \leq 0.05$, $|d| < 0.147$). When the ventilation rate is set at 6 air changes per hour (as shown in

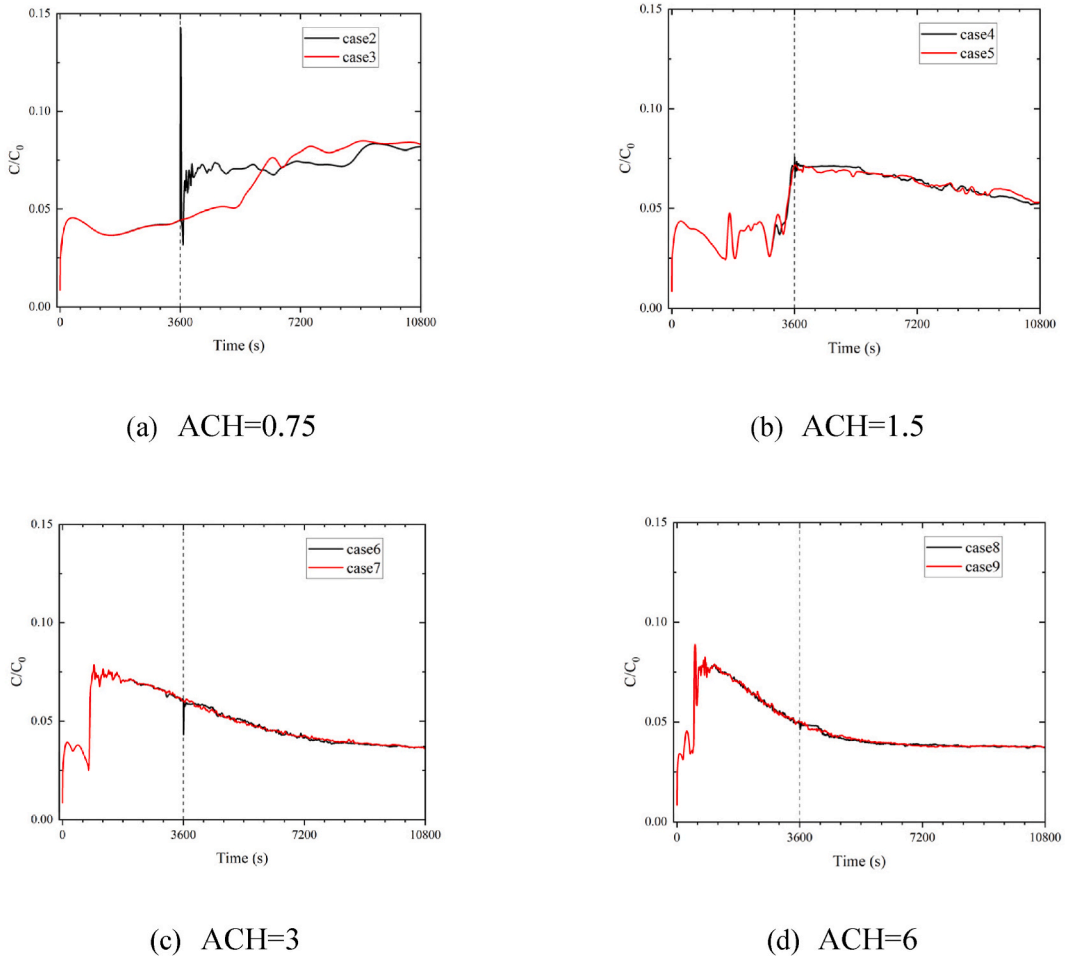

Fig. 7. Impact of Ventilation and Door Conditions on Relative Average Concentration at Sensor1 (The start time corresponds to the t = 43200 in cases above).

Fig. 7(d)), the door operations have no significant impact on the airflow field ($p > 0.05$, $|d| < 0.147$).

In the study of airflow characteristics, the opening and closing process of doors have a significant influence on the airflow behavior. Considering case 2, Fig. 8(a) illustrates the situation during the 4-s period when the door transitions from a closed state to a 45-degree open state. During this period, the airflow velocity increases, and a low-pressure region is formed in the area after the door is opened, promoting the movement of airflow from high-pressure areas to low-pressure areas. A large amount of indoor airflow flows out of the isolation room through the open door, creating a vortex that appears in the area outside the bedroom opposite to the direction of door opening, with the main airflow direction being westward and southward. Fig. 8(b) depicts the situation during a 7-s period when the door remains open. During this time, the outflow of indoor airflow decreases, and the previously formed vortex migrates and expands towards the exit boundary, while a new vortex forms on the northern side. Fig. 8(c) presents the situation during the 4-s period when the door transitions from the open state to the closed state. Due to the obstruction of the airflow outlet, the indoor air pressure correspondingly increases, and the vortex on the southern side continues to expand. Therefore, this study can infer that the opening and closing actions of the door significantly affect the organizational morphology of the airflow field, further influencing the dispersion and distribution patterns of aerosols.

4.3. Infection risk assessment

Fig. 9 depicts the infection risk in various regions outside the bedroom during an extended 12-h period of indoor non-ventilation. The results indicate that the overall infection risk in the monitored regions is exceptionally low and can be disregarded. While there is a slight elevation in infection risk near the proximity of the bedroom door, the likelihood of infection remains exceedingly low. Consequently, under conditions of inadequate indoor ventilation in the isolation room, the extended presence and activities of individuals in the outdoor environment pose a highly minimal risk of infection.

The infection risk in different regions for cases 2 to 9 was computed and presented in Figs. 10 and 1(a) to (d) show the infection risks of ACH = 0.75, 1.5, and 3.6 in different regions. Through hypothesis testing, this study observed statistically significant differences in the impact of door opening and closing actions on the infection risk, although the effect size was relatively small when considering the same ventilation rate ($p \leq 0.05$, $|d| \leq 0.2$). Consequently, when evaluating the infection risk in diverse regions, this study selected representative cases that encompassed door opening and closing actions, namely cases 2, 4, 6, and 8, for subsequent analysis. The infection risk was calculated using a dose-response model as detailed in Section 2.4. This model links pathogen exposure to infection risk by considering factors such as aerosol size, spatial heterogeneity, and time-varying infection probabilities.

From an overall perspective, when considering the same ventilation rate, there are minimal differences in the spatially averaged infection risk among various regions ($p \leq 0.05$, U test; $|d| \leq 0.2$). Increasing the ventilation rate leads to a slight elevation of approximately 10 % in the infection risk across all regions and reduces the duration of low infection probability from an average of 5000s to an average of 4500s. In cases where the bedroom maintains a specific ventilation rate, the average infection risk for individuals who partake in prolonged activities in the external regions of the bedroom amounts to approximately 60 %, indicating a high probability of occurrence. Therefore, in scenarios where there are isolated patients residing in the bedroom for extended durations while healthy individuals conduct activities in the surrounding communal areas, it is not advisable to maintain ventilation within the bedroom to mitigate the influence of the bedroom door on infection risk. However, in situations where ventilation is upheld within the master bedroom and healthy individuals require engagement in activities within the shared spaces outside the bedroom, it is recommended to limit the duration of continuous activity to no more than 75 min to uphold a lower infection risk.

Among the four designated regions, the living room (Livingroom) area demonstrates the highest susceptibility to infection, followed by the dining room area (Diningroom), whereas the near-door area (Neardoor) outside the bedroom exhibits the lowest susceptibility. The overall infection risk in the vicinity of the bedroom is comparable to that observed in the dining room area. This

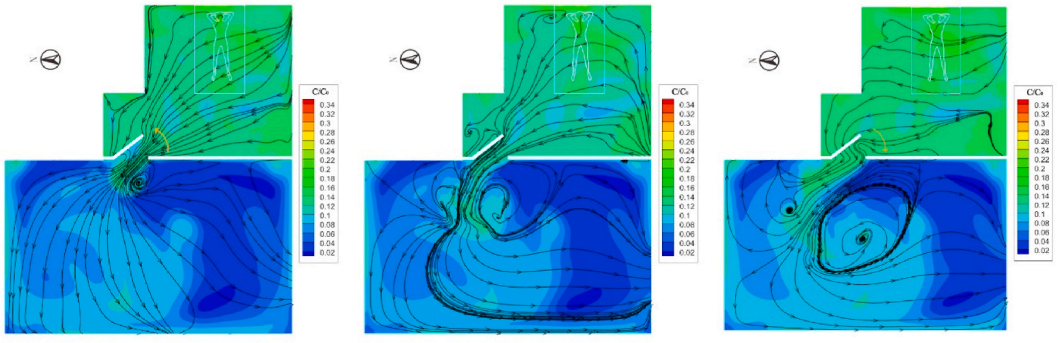

(a) Flow field during door opening process (b) Flow field during door opening (c) Flow field during door closing process

Fig. 8. Flow field during the opening and closing process at a height of z = 0.7m in case2.

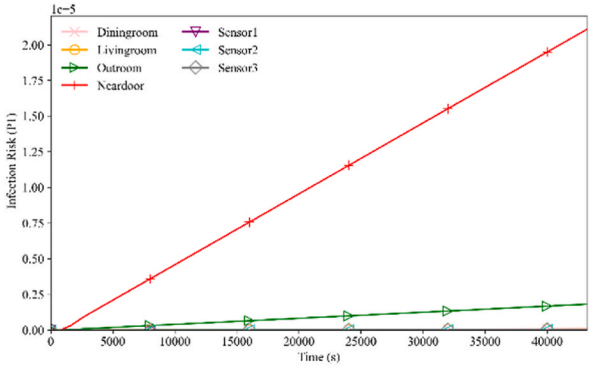

Fig. 9. Infection risk with no Ventilation.

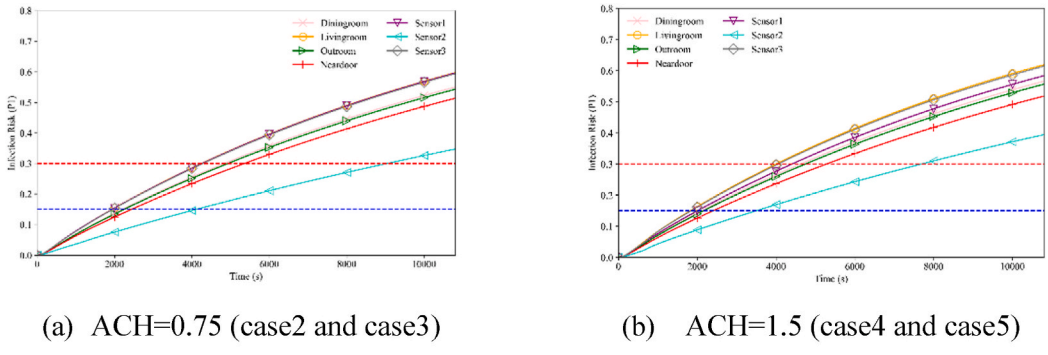

(a) ACH=0.75 (case2 and case3) (b) ACH=1.5 (case4 and case5)

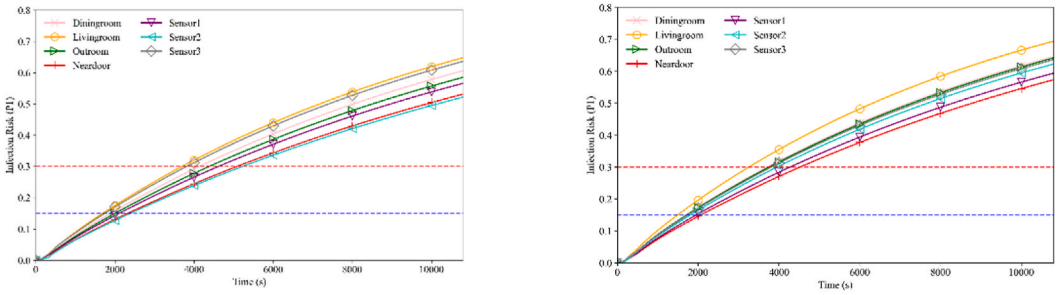

(c) ACH=3 (case6 and case7) (d) ACH=6 (case8 and case9)

Fig. 10. Impact of Ventilation Rates on Infection risk.

observed phenomenon can be attributed to the living room area's position in the downwind direction of the airflow and its proximity to expansive wall surfaces, which facilitate aerosol accumulation. Despite the near-door area outside the master bedroom being in close proximity to the pollution source, its open spatial configuration enhances aerosol clearance efficacy.

In cases with lower ventilation rates, such as case 2 and case 3, there is a significant disparity between the infection probabilities at sensor 2 and the infection probabilities based on spatially averaged regions. This disparity is not observed in cases with higher ventilation rates, indicating that at lower ventilation rates, the aerosols in the airflow do not achieve uniform mixing, and the infection risk is strongly influenced by an individual's location. Therefore, a more precise analysis of overall infection risk needs to consider individual behavior trajectories. However, at other monitoring points, the infection risk is highly similar to the overall infection risk in their respective nearby regions. This suggests that, under limited measurement conditions, utilizing the infection risk at monitoring points as representative of the infection risk for a specific region is feasible.

5. Conclusion and limitation

This research employed numerical simulations to delve into the characteristics of aerosol transmission inside and outside isolation rooms, as well as the risk of infection posed by individuals in home isolation to healthy individuals outdoors. Initially, this study conducted an analysis of the spatial distribution of aerosol concentrations outside the isolation rooms based on time-averaged data, along with an investigation of airflow patterns. Subsequently, this study examined the influence of ventilation conditions, door leakage, and door opening/closing operations on aerosol concentrations and infection risks in different regions of the airflow. Furthermore, this study explored the correlation between aerosol concentrations in various areas and their corresponding infection risks, while also assessing the variations in infection risks under different ventilation conditions. Ultimately, this study derived practical recommendations based on our study findings and proposed potential avenues for future research. In essence, this study contributes significant insights in the following aspects:

1. Overall, under specific ventilation conditions, both door leakage and door opening/closing actions can lead to varying degrees of indoor aerosol transmission into the adjacent area neighboring the isolation room, thereby posing a certain level of exposure risk to individual. The magnitude of the risk mainly dependents on the ventilation rate in the isolation room and the duration of individuals' stay.
2. In the absence of ventilation, door leakage has minimal impact on aerosol concentrations in the adjacent area neighboring the isolation room, resulting in infection risks lower than 2×10^{-5}.
3. Under ventilated conditions, the infection risk of people in adjacent room was significantly correlated with residence time. If individuals spend more than 3 h in that area, the average infection risk in the adjacent area may exceed 60 %.
4. Overall infection risk is minimally influenced by ventilation rates. For example, when ventilation rate increases from 0.75 to 6 air changes per hour, the infection risk rises from 55 % to 65 % after 3 h. This may seem counterintuitive, since higher ventilation rates do help disperse aerosols, but they also allow infected aerosols to spread more quickly into adjacent Spaces.
5. At lower ventilation rates, door opening/closing actions have a significant impact on the airflow, potentially causing transient peaks in aerosol concentrations. However, when the ventilation rate is equal to or greater than 1.5 air changes per hour, it diminishes. And aerosol leakage between adjacent rooms primarily occurs through door gap instead of door actions. This finding aligns with previous studies which have also found that door gaps are major pathways for aerosol leakage. Studies by Pantelic et al. have shown that even small gaps around doors can allow significant aerosol transfer, especially at low ventilation rates [52].
6. With ventilation, the area near downwind walls opposite the door in the adjacent room has the highest aerosol and infection risk; without ventilation, it's the area close to the door.

In summary, this study extensively investigates the characteristics of aerosol transmission between indoor and adjacent areas in isolation settings, as well as its implications for infection risk. The findings provide valuable insights for the development of practical control measures. Based on the results, the following recommendations are suggested for real-world scenarios:

1. Setting up an isolation area within a confined space is a secure method for home isolation. Under such circumstances, the risk of infection for individuals in the adjacent area can be considered negligible.
2. When the isolation room is ventilated, in order to maintain the infection risk below 30 %, it is advised to avoid prolonged stays in the adjacent area exceeding 75 min. To reduce the infection risk to 15 %, it is recommended to avoid prolonged stays in the adjacent area exceeding 35 min.
3. In the scenario of home isolation where frequent opening and closing of the isolation room door is necessary, it is recommended to ensure a ventilation rate within the isolation room of equal to or greater than 1.5 air changes per hour in order to ensure the safety of individuals in the adjacent area.
4. In the context of home isolation, individuals in the adjacent area should preferably engage in activities in open spaces, avoiding areas near downwind walls.
5. When designing isolation rooms for epidemic prevention purposes, the size of the door gap is crucial. It is advisable to select isolation room doors with better sealing performance.

However, to facilitate numerical simulations, this study has simplified the aerosol transmission process between the isolation room and the outside environment to some extent. For example, it assumed uniform distribution of aerosol particles and neglected the impact of indoor furniture, human presence, and other objects on the airflow field. These simplifications may affect the accuracy of the simulation results. Furthermore, this study only considered a common household layout in Wuhan. Additionally, the study assumes constant outdoor wind speed, a significant simplification given that variations in wind conditions can substantially impact aerosol dynamics and ventilation strategies. Higher wind speeds might enhance ventilation, reducing indoor aerosol accumulation, while lower wind speeds could lead to less efficient ventilation and higher concentrations. In real-time applications, these dynamic environmental conditions can influence the effectiveness of aerosol management strategies. Recognizing this, future studies should incorporate variable wind conditions and more diverse building layouts and climatic factors to better understand how these variables influence aerosol transmission. This approach would make the simulation results more applicable to a broader range of scenarios and more reflective of real-time environmental changes.

Moreover, using a dose-response model for influenza A to calculate infection risk for COVID-19 has limitations due to differences in pathogen characteristics, transmission dynamics, and infection mechanisms. While the influenza A model provides a framework, it

may not fully capture the specifics of COVID-19 transmission. The assumption that the characteristics of influenza A are comparable to those of COVID-19 simplifies the modeling process but introduces inaccuracies. Future work will focus on developing dose-response models specific to COVID-19, incorporating data on its aerosol behavior, infectious dose, and transmission characteristics. Additionally, validating these models with experimental and epidemiological data specific to COVID-19 would enhance their accuracy and reliability. Exploring multi-pathogen models that can adapt to various respiratory diseases could also be a valuable direction for improving infection risk assessments.

Lastly, these simplifications could lead to inaccuracies in predicting aerosol behavior, as real-world scenarios often involve non-uniform particle distributions and complex interactions with furniture and occupants. Such factors can create localized airflow patterns and areas of higher or lower aerosol concentration that are not captured in the simulations. Future research can improve the accuracy and applicability of the simulation results by incorporating more realistic factors, such as the presence of furniture, varying occupant activities, and different room layouts. Experimental validation with real-world data can also help refine the models and improve their reliability, bridging the gap between theoretical simulations and practical, real-world applications.

Ethical statement

This study involved the distribution of questionnaires to collect data. Since no personal or sensitive data was collected, and the study posed no risk to participants, ethical approval was not required. Participation in the survey was entirely voluntary, and informed consent was obtained from all participants. Participants were informed of the purpose of the study, assured of the confidentiality of their responses, and were free to withdraw at any time without consequence.

Data availability statement

The data generated and analyzed during this study are available from the corresponding author on reasonable request. Since the study involved questionnaire responses, no specific datasets were deposited in a public repository. Any additional information regarding the data can be provided upon request to ensure transparency and reproducibility of the results.

CRediT authorship contribution statement

Xunmei Wu: Writing – review & editing, Writing – original draft, Conceptualization. **Mengtao Han:** Supervision, Software, Resources, Methodology, Funding acquisition. **Hong Chen:** Funding acquisition, Conceptualization.

Declaration of competing interest

The authors declare that they have no known competing financial interests or personal relationships that could have appeared to influence the work reported in this paper.

Acknowledgments

This study was supported by the National Natural Science Foundation of China No. 51778251 and the National Natural Science Foundation of China Project No. 52208059. Numerical computations were performed on the Hefei Advanced Computing Center.

Appendix A. Validation of the LBM-LES model

The two-room model used in this study was derived from the experiments conducted by Alvin [53] and has been previously employed to validate other indoor air quality issues. As shown in Figure A1, the model has dimensions of 0.8 m in length, 0.4 m in width, and 0.4 m in height. The large opening divides the room into two sections, with spatial symmetry on either side of the opening. The opening is centrally symmetric about the center plane, with a width (y) of 0.08 m and a height (z) of 0.24 m. The inlet and outlet sizes are identical and positioned 2 cm away from the ceiling and floor, respectively. The inlet velocity is set at 0.225 m/s, and the air change rate (ACH) is 10^{-1}, based on a Reynolds number of 600 calculated from previous research by Posner in 2003, which serves as the scaling standard for Reynolds number. The room air is initially clean, and particles are continuously supplied at a constant rate along with the inlet air. The particle size is 10 μm, with a particle density of approximately 1550 kg/mˆ3. The simulation time using the lattice Boltzmann method (LBM) and finite volume method (FVM) is 900 s, followed by a 100-s time averaging process.

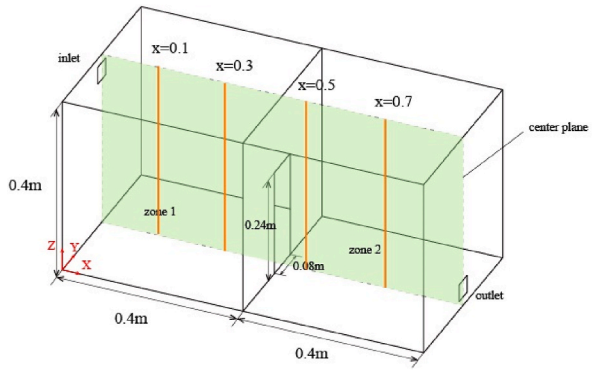

Fig. A1Schematic Diagram of the Computational Domain

In order to compare the particle velocities and concentrations within the two-zone model indoor environment, the concept of relative concentration is introduced in this chapter, with the concentration at the inlet set as 1. Figure A2 presents a comparison between measured and predicted values of velocity and particle concentration along the x-direction. The simulation predictions exhibit a similar overall trend to the experimental data and show a good agreement, except for the region near the floor where the measured velocity is nearly zero. The overall trend of particle concentration matches well with the predicted trend from the numerical model. In the second zone of the two-zone indoor environment, only a small number of particles is detected, indicating that the concentration in these areas is nearly negligible. The Lattice Boltzmann Method (LBM) simulation generates higher relative concentrations near the bottom of the indoor environment, which can be attributed to the influence of particle density and the strong settling effect observed in the particles. Overall, both LBM-LES and FVM-LES demonstrate consistent performance, effectively capturing the flow characteristics. The simulation data in this study closely aligns with both the experimental and simulated data, indicating that the lattice Boltzmann method can accurately simulate the flow field and particle distribution in a ventilated indoor environment. Our model validation is based on previous study, where the FVM method was validated against experimental data using FLUENT. Given that the FVM method is widely used and accepted, this provides a strong basis for validating our LBM-LES approach.

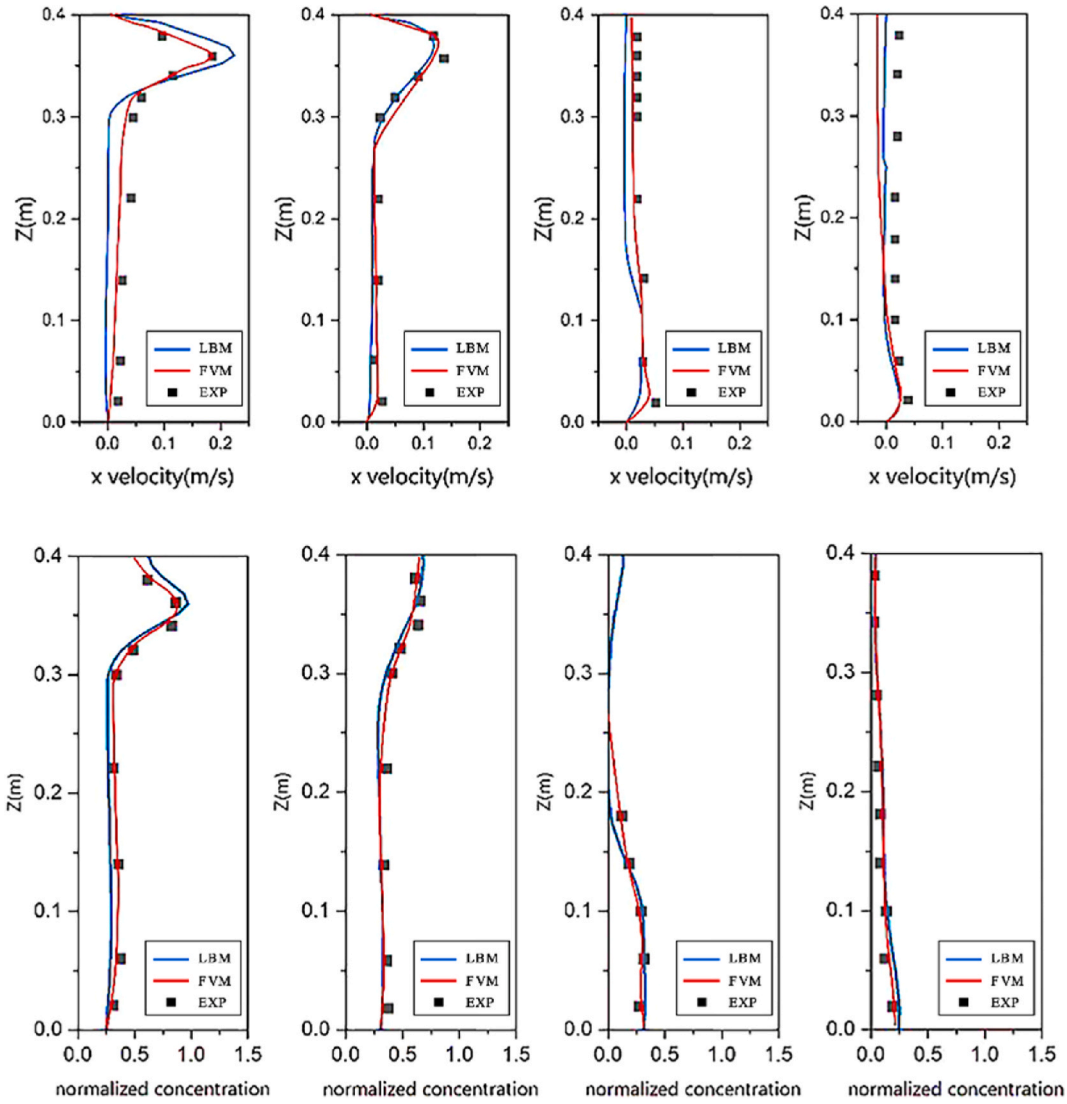

Fig. A2. Comparison of velocity and particle concentration between measured and predicted values

Appendix B. Boundary condition determination

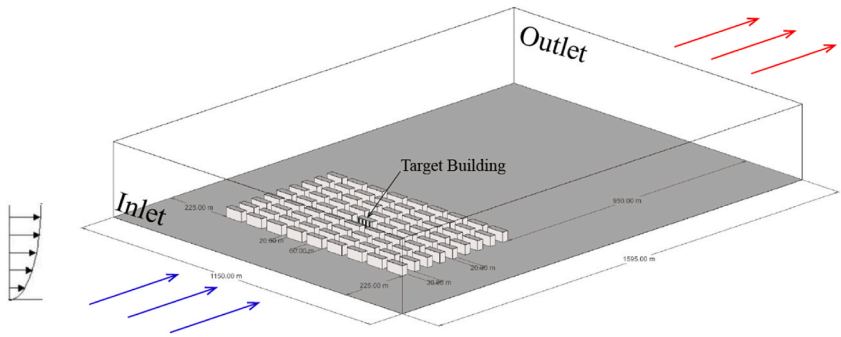

Fig. B1. Computational domain of street block

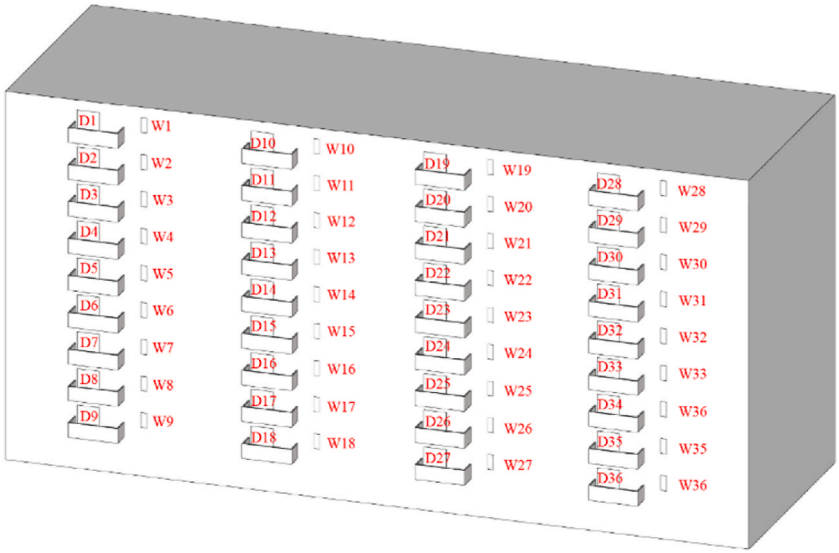

Fig. B2. Target building facade and doors and windows numbering

Table B1
Static pressure of each pair of doors and windows on the facade

ID	static pressure (D)	static pressure (W)	Difference	ID	static pressure (D)	static pressure (W)	Difference
1	−1.95253	−1.71727	−0.23526	19	0.709587	0.724362	−0.01478
2	0.087732	0.02428	0.063452	20	−1.68719	1.208817	−2.89601
3	0.155611	0.059741	0.09587	21	−0.46868	−0.30679	−0.16189
4	1.064238	0.745515	0.318723	22	−0.72756	−0.50309	−0.22447
5	0.010251	0.071786	−0.06154	23	−0.80788	−0.63612	−0.17176
6	−0.22118	0.43837	−0.65955	24	−0.79882	−0.68825	−0.11057
7	−0.04239	−0.03741	−0.00498	25	−0.90486	−0.68718	−0.21768
8	−0.6091	−0.41631	−0.19278	26	−0.80946	−0.70875	−0.10071
9	−0.7027	−0.5951	−0.1076	27	−0.84801	−0.71665	−0.13136
10	1.797581	−0.50901	2.306586	28	−0.8815	−0.59483	−0.28668
11	0.285931	−0.28006	0.565995	29	−0.92275	−0.56649	−0.35626
12	−0.12317	−0.05169	−0.07149	30	−1.05548	−0.77934	−0.27614
13	−0.27972	−0.07229	−0.20743	31	−1.14952	−0.92155	−0.22797
14	−4.05484	−6.96414	2.9093	32	−1.20437	−0.99347	−0.2109
15	−5.35899	−6.14732	0.78833	33	−1.15386	−1.11992	−0.03393
16	−0.06215	−0.05461	−0.00754	34	−0.95443	−1.16742	0.212986
17	−0.07006	−0.05198	−0.01809	35	−1.05104	−0.93286	−0.11817
18	−0.07594	−0.07448	−0.00146	36	−0.88193	−0.95278	0.070856

As mentioned in Section 3.2, to clarify the impact of the balcony on airflow disturbance, this study positioned a residential building in the center of a homogeneous urban block. All units within the building adhere to the typical layout found in Wuhan, as identified through clustering methods. Considering the prevailing southerly wind direction in Wuhan [54], the computational domain's inlet is oriented due south with an adequate wake area. The simulation utilized approximately 1.6 million grids and employed the RNG k-ε model. Both the building surfaces and the ground are treated as wall boundaries, the sky is modeled with moving wall boundary, and the lateral boundaries are symmetric. The inlet uses an urban gradient wind boundary, and the outlet is set as an outflow boundary. The specific dimensions of the computational domain are shown in Figure B1.

Figure B2 presents the facade of the building, with all the sliding doors connected to living room balconies (facing west) and bedroom windows (also facing west) labeled and numbered. The naming convention for the sliding doors is 'D' (door) followed by a numerical identifier, and for the bedroom windows, it is 'W' (window) followed by a numerical identifier, as detailed in Table B1. Among the 36 units, 28 units show lower static pressure at the sliding door side compared to the bedroom window side, suggesting that airflow enters through the bedroom windows and exits through the living room sliding doors. This airflow pattern is likely influenced by turbulence caused by the balcony, allowing us to model the bedroom window as a relatively positive pressure inlet boundary. With an average pressure difference of 0.006253pa across the 36 pairs of windows and doors, the ideal flow velocity under this pressure differential can be calculated using Bernoulli's equation (equation (B1)) :

$$v = \sqrt{\frac{2\Delta P}{\rho}} \tag{B1}$$

In equation, v represents the fluid's velocity, ΔP is the static pressure difference between two points, measured in Pascals (Pa), which

serves as the driving force for fluid movement from one location to another. The density of the fluid, ρ is measured in kilograms per cubic meter (kg/m^3). Under standard conditions, the density of air is approximately 1.225 kg/m^3. Using equation (B1), the inlet velocity of air through the bedroom window is approximately 0.1012 m/s. This result is remarkably close to the findings by Xiong et al. [55], who observed an airflow velocity of 0.1008 m/s at a window of a single-sided ventilated room near a Wuhan Street canyon under strong wind conditions (wind speed of 3 m/s).

References

[1] C.-C. Hsieh, C.-H. Lin, W.Y.C. Wang, D.J. Pauleen, J.V. Chen, The outcome and implications of public precautionary measures in Taiwan–Declining respiratory disease cases in the COVID-19 pandemic, Int. J. Environ. Res. Publ. Health 17 (2020) 4877.
[2] C.M. Long, H.H. Suh, P.J. Catalano, P. Koutrakis, Using time-and size-resolved particulate data to quantify indoor penetration and deposition behavior, Environ. Sci. Technol. 35 (2001) 2089–2099.
[3] D. Huremović, Social distancing, quarantine, and isolation, Psychiatry of Pandemics: A Mental Health Response to Infection Outbreak (2019) 85–94.
[4] L. Morawska, Environmental Aerosol Physics, Queensland University of Technology, Brisbane, 2003.
[5] N.S. Holmes, L. Morawska, A review of dispersion modelling and its application to the dispersion of particles: an overview of different dispersion models available, Atmos. Environ. 40 (2006) 5902–5928.
[6] L. Morawska, G.R. Johnson, Z.D. Ristovski, M. Hargreaves, K. Mengersen, S. Corbett, C.Y.H. Chao, Y. Li, D. Katoshevski, Size distribution and sites of origin of droplets expelled from the human respiratory tract during expiratory activities, J. Aerosol Sci. 40 (2009) 256–269.
[7] C. Liu, S. Shi, C. Weschler, B. Zhao, Y. Zhang, Analysis of the dynamic interaction between SVOCs and airborne particles, Aerosol. Sci. Technol. 47 (2013) 125–136.
[8] M. Nicas, G. Sun, An integrated model of infection risk in a health-care environment, Risk Anal. 26 (2006) 1085–1096.
[9] M. Nicas, R.M. Jones, Relative contributions of four exposure pathways to influenza infection risk, Risk Analysis, Int. J. 29 (2009) 1292–1303.
[10] M. Nicas, W.W. Nazaroff, A. Hubbard, Toward understanding the risk of secondary airborne infection: emission of respirable pathogens, J. Occup. Environ. Hyg. 2 (2005) 143–154.
[11] M.A. Cava, K.E. Fay, H.J. Beanlands, E.A. McCay, R. Wignall, The experience of quarantine for individuals affected by SARS in Toronto, Publ. Health Nurs. 22 (2005) 398–406.
[12] M.O. Elgendy, M.N. Abd Elmawla, A.M. Abdel Hamied, S.O. El Gendy, M.E.A. Abdelrahim, COVID-19 patients and contacted person awareness about home quarantine instructions, Int. J. Clin. Pract. 75 (2021) e13810.
[13] Z. Guo, D. Xiao, Epidemiological analysis of asymptomatic SARS-CoV-2 transmission in the community: an individual-based model, Sci. Rep. 11 (2021) 6251.
[14] R. Zhang, Y. Wang, Z. Lv, S. Pei, Evaluating the impact of stay-at-home and quarantine measures on COVID-19 spread, BMC Infect. Dis. 22 (2022) 1–13.
[15] E.-A. Kim, Social distancing and public health guidelines at workplaces in Korea: responses to coronavirus disease-19, Saf Health Work 11 (2020) 275–283.
[16] M.L. Geisinger, E. Iaonnidou, Up in the air? Future research strategies to assess aerosols in dentistry, JDR Clin. Trans. Res. 6 (2021) 128–131.
[17] L. Chang, X. Zhang, S. Wang, J. Gao, Control room contaminant inleakage produced by door opening and closing: dynamic simulation and experiments, Build. Environ. 98 (2016) 11–20.
[18] A. Hathway, I. Papakonstantis, A. Bruce-Konuah, W. Brevis, Experimental and modelling investigations of air exchange and infection transfer due to hinged-door motion in office and hospital settings, Int. J. Vent. 14 (2015) 127–140.
[19] J.F.S.J. Alonso, M.A. Sanz-Tejedor, Y. Arroyo, M.R. San José-Gallego, Analysis and assessment of factors affecting air inflow from areas adjacent to operating rooms due to door opening and closing, J. Build. Eng. 49 (2022) 104109.
[20] L. Fontana, A. Quintino, Experimental analysis of the transport of airborne contaminants between adjacent rooms at different pressure due to the door opening, Build. Environ. 81 (2014) 81–91.
[21] P. Zhao, Q. Li, S.B. Kuang, Z. Zou, LBM-LES simulation of the transient asymmetric flow and free surface fluctuations under steady operating conditions of slab continuous casting process, Metall. Mater. Trans. B 48 (2017) 456–470.
[22] H. Sajjadi, M. Salmanzadeh, G. Ahmadi, S. Jafari, Turbulent indoor airflow simulation using hybrid LES/RANS model utilizing Lattice Boltzmann method, Comput. Fluids 150 (2017) 66–73.
[23] M. Han, R. Ooka, H. Kikumoto, Effects of wall function model in lattice Boltzmann method-based large-eddy simulation on built environment flows, Build. Environ. 195 (2021) 107764.
[24] H. Chen, X. Wu, M. Han, Y. Zhang, Impacts of solid wall boundary conditions in the lattice Boltzmann method on turbulent outdoor flow: a case study of a single 1: 1: 2 building model, Build. Environ. 226 (2022) 109708.
[25] S. Chen, G.D. Doolen, Lattice Boltzmann method for fluid flows, Annu. Rev. Fluid Mech. 30 (1998) 329–364.
[26] P. Lallemand, L.-S. Luo, Theory of the lattice Boltzmann method: dispersion, dissipation, isotropy, Galilean invariance, and stability, Phys. Rev. E 61 (2000) 6546.
[27] P. Van Leemput, W. Vanroose, D. Roose, Initialization of a lattice Boltzmann model with constrained runs (Extended Version), Katholieke Universiteit Leuven, Report TW 444 (2005).
[28] M. Murakami, T.L. Clark, W.D. Hall, Numerical simulations of convective snow clouds over the sea of Japan two-dimensional simulations of mixed layer development and convective snow cloud formation, Journal of the Meteorological Society of Japan. Ser. II 72 (1994) 43–62.
[29] A.C.K. Lai, W.W. Nazaroff, Modeling indoor particle deposition from turbulent flow onto smooth surfaces, J. Aerosol Sci. 31 (2000) 463–476.
[30] J.A. Gliner, N.L. Leech, G.A. Morgan, Problems with null hypothesis significance testing (NHST): what do the textbooks say? J. Exp. Educ. 71 (2002) 83–92.
[31] B. Rosner, R.J. Glynn, Power and sample size estimation for the Wilcoxon rank sum test with application to comparisons of C statistics from alternative prediction models, Biometrics 65 (2009) 188–197.
[32] G. Macbeth, E. Razumiejczyk, R.D. Ledesma, Cliff's Delta Calculator: a non-parametric effect size program for two groups of observations, Universitas Psychologica 10 (2011) 545–555.
[33] L. Desquilbet, F. Mariotti, Dose-response analyses using restricted cubic spline functions in public health research, Stat. Med. 29 (2010) 1037–1057.
[34] G.N. Sze To, C.Y.H. Chao, Review and comparison between the Wells–Riley and dose-response approaches to risk assessment of infectious respiratory diseases, Indoor Air 20 (2010) 2–16.
[35] S.T. Gn, M.P. Wan, C.Y. Chao, F. Wei, S.C. Yu, J.K. Kwan, A methodology for estimating airborne virus exposures in indoor environments using the spatial distribution of expiratory aerosols and virus viability characteristics, Indoor Air 18 (2008) 425–438.
[36] B.R. Murphy, E.G. Chalhub, S.R. Nusinoff, J. Kasel, R.M. Chanock, Temperature-sensitive mutants of influenza virus. III. Further characterization of the ts-1 [E] influenza A recombinant (H3N2) virus in man, JID (J. Infect. Dis.) 128 (1973) 479–487.
[37] J.H. Hemmes, K. Winkler, S.M. Kool, Virus survival as a seasonal factor in influenza and poliomyelitis, Nature 188 (1960) 430–431.
[38] R.H. Alford, J.A. Kasel, P.J. Gerone, V. Knight, Human influenza resulting from aerosol inhalation, PSEBM (Proc. Soc. Exp. Biol. Med.) 122 (1966) 800–804.
[39] C. Xu, P. V Nielsen, G. Gong, R.L. Jensen, L. Liu, Influence of air stability and metabolic rate on exhaled flow, Indoor Air 25 (2015) 198–209.
[40] L. Morawska, G.R. Johnson, Z.D. Ristovski, M. Hargreaves, K. Mengersen, S. Corbett, C.Y.H. Chao, Y. Li, D. Katoshevski, Size distribution and sites of origin of droplets expelled from the human respiratory tract during expiratory activities, J. Aerosol Sci. 40 (2009) 256–269.
[41] M. Rausand, in: Theory, Method and Application of Risk Assessment 2, 2013, pp. 101–105.

[42] J. Wilpon, L. Rabiner, A modified K-means clustering algorithm for use in isolated work recognition, IEEE Trans. Acoust. 33 (1985) 587–594.
[43] S. Holm, A general approach to compensation for losses incurred due to public health interventions in the infectious disease context, Monash Bioeth. Rev. 38 (2020) 32–46.
[44] E. Simiu, D. Yeo, Wind Effects on Structures: Modern Structural Design for Wind, John Wiley & Sons, 2019.
[45] Y. Nonomura, N. Kobayashi, Y. Tominaga, A. Mochida, The cross comparison of CFD results forflow field around building models (Part 3)-Wind tunnel test for the verification of models for the flow field around building blocks, in: Summaries of Technical Papers of Annual Meeting, Japan Association for Wind Engineering, 2003, pp. 83–84.
[46] F. Nicoud, F. Ducros, Subgrid-scale stress modelling based on the square of the velocity gradient tensor, Flow, Turbul. Combust. 62 (1999) 183–200.
[47] C. Orr Jr., F.K. Hurd, W.J. Corbett, Aerosol size and relative humidity, J. Colloid Sci. 13 (1958) 472–482.
[48] K.N. Premnath, J. Abraham, Three-dimensional multi-relaxation time (MRT) lattice-Boltzmann models for multiphase flow, J. Comput. Phys. 224 (2007) 539–559.
[49] M. Hecht, J. Harting, Implementation of on-site velocity boundary conditions for D3Q19 lattice Boltzmann simulations, J. Stat. Mech. Theor. Exp. 2010 (2010). P01018.
[50] Y. Xiong, H. Chen, Effects of sunshields on vehicular pollutant dispersion and indoor air quality: comparison between isothermal and nonisothermal conditions, Build. Environ. 197 (2021) 107854.
[51] J. Van Strien, K. Shrestha, S. Gabriel, P. Lappas, D.F. Fletcher, N. Singh, K. Inthavong, Pressure distribution and flow dynamics in a nasal airway using a scale resolving simulation, Phys. Fluids 33 (2021) 011907.
[52] J. Pantelic, K.W. Tham, D. Licina, Effectiveness of a personalized ventilation system in reducing personal exposure against directly released simulated cough droplets, Indoor Air 25 (2015) 683–693.
[53] A.C.K. Lai, K. Wang, F.Z. Chen, Experimental and numerical study on particle distribution in a two-zone chamber, Atmos. Environ. 42 (2008) 1717–1726.
[54] J. Lei, L. Liu, X. Luan, W. Wan, Model study on neutral winds in the ionospheric F-region and com-parison with the equivalent winds derived from the wuhan ionosonde data, TAO 14 (2003) 1–12.
[55] Y. Xiong, H. Chen, Effects of sunshields on vehicular pollutant dispersion and indoor air quality: comparison between isothermal and nonisothermal conditions, Build. Environ. 197 (2021) 107854.